Cell, Vol. 85, 707–720, May 31, 1996, Copyright ©1996 by Cell Press

Mice Lacking p27^{Kip1} Display Increased Body Size, Multiple Organ Hyperplasia, Retinal Dysplasia, and Pituitary Tumors

Keiko Nakayama,*‡ Noriko Ishida,* Michiko Shirane,* Akira Inomata,† Tomoaki Inoue,† Nobuyuki Shishido,† Ikuo Horii,† Dennis Y. Loh,*‡ and Kei-ichi Nakayama*‡
*Department of Biology
†Department of Toxicology and Pathology
Nippon Roche Research Center
Kamakura
Kanagawa 247
Japan
‡Howard Hughes Medical Institute
Department of Medicine, Genetics, and Molecular Microbiology
Washington University School of Medicine
St. Louis, Missouri 63110

Summary

Mice lacking p27^{Kip1} have been created by gene targeting in embryonic stem cells. These mice are larger than the control animals, with thymus, pituitary, and adrenal glands and gonadal organs exhibiting striking enlargement. CDK2 activity is elevated about 10-fold in p27$^{-/-}$ thymocytes. Development of ovarian follicles seems to be impaired, resulting in female sterility. Similar to mice with the *Rb* mutation, the p27$^{-/-}$ mice often develop pituitary tumors spontaneously. The retinas of the mutant mice show a disturbed organization of the normal cellular layer pattern. These findings indicate that p27^{Kip1} acts to regulate the growth of a variety of cells. Unexpectedly, the cell cycle arrest mediated by TGFβ, rapamycin, or contact inhibition remained intact in p27$^{-/-}$ cells, suggesting that p27^{Kip1} is not required in these pathways.

Introduction

A series of cyclin and cyclin-dependent kinase (CDK) complexes plays a central role in the regulation of cell cycle progression (reviewed by Sherr, 1994; Hunter and Pines, 1994). In mammalian cells, the cyclin D–CDK4 and cyclin E–CDK2 complexes are catalytically active during late G1 phase and are implicated in the regulation of G1/S progression. The retinoblastoma protein (pRb), the first identified oncosuppressor product, is one of their putative substrates, and phosphorylation of pRb appears to inactivate its ability to inhibit transactivation of certain transcription factors that are important for cell cycle control (reviewed by Weinberg, 1995). Another oncosuppressor gene product, p53, is also involved in the control of G1/S phase progression by regulating the gene expression of p21^{Cip1} (also known as Waf1, Sdi1, or CAP20). p21^{Cip1} was the first of a group of proteins identified as CDK inhibitors. These proteins all block the kinase activity of cyclin–CDK complexes (El-Deiry et al., 1993; Harper et al., 1993; Xiong et al., 1993; Gu et al., 1993; Noda et al., 1994) and include p27^{Kip1} (Toyoshima and Hunter, 1994; Polyak et al., 1994b), p57^{Kip2} (Matsuoka et al., 1995; Lee et al., 1995), p16^{Ink4A} (Serrano et al., 1993), p15^{Ink4B} (Hannon and Beach, 1994), p18^{Ink4C} (Guan et al., 1994; Hirai et al., 1995), and p19^{Ink4D} (Chan et al., 1995; Hirai et al., 1995). CDK inhibitors are classified into two families. The Cip/Kip family members (p21, p27, and p57) possess the ability to inhibit a variety of cyclin–CDK complexes and share partial structural similarity. The Ink4 family members (p16, p15, p18, and p19) are CDK4/CDK6-specific inhibitors. All CDK inhibitors cause G1 arrest when overexpressed in transfected cells (reviewed by Sherr, 1994; Sherr and Roberts, 1995).

Cell proliferation is precisely controlled by growth-stimulatory and growth-inhibitory signals transduced from the extracellular environment. Because some of the inhibitory signals are believed to be mediated by CDK inhibitors, it is possible that these molecules contribute to cell cycle exit during differentiation. Consistent with this hypothesis, p21^{Cip1} is induced in cell lines undergoing differentiation in vitro (Jiang et al., 1994; Steinman et al., 1994; Noda et al., 1994; Parker et al., 1995; Halevy et al., 1995) and is expressed in vivo during embryogenesis, primarily in a subset of cells that are amitotic (Parker et al., 1995). Recently, however, it was shown that p21^{Cip1}-deficient mice undergo normal development, but fibroblasts from these mice are defective in G1 arrest in response to DNA damage and nucleotide pool perturbation (Deng et al., 1995; Brugarolas et al., 1995). However, in response to γ-irradiation, the G1 checkpoint is only partially impaired, indicating the existence of a second p53-dependent function capable of arresting the cell cycle in G1. In addition, unlike the p53$^{-/-}$ animals, p21$^{-/-}$ mice do not exhibit early tumorigenesis or an inability to induce apoptosis. Consistent with this experimental animal model is the failure to find mutations in the p21^{Cip1} gene in human tumors (Shinohara et al., 1994).

p27^{Kip1} is associated predominantly with cyclin D–CDK4, but shows the ability to inhibit a variety of cyclin–CDK complexes in vitro (Toyoshima and Hunter, 1994; Polyak et al., 1994b). p27^{Kip1} shares homology with p21^{Cip1} and p57^{Kip2} at the N-terminal domain (CDK-binding/inhibitory domain). Several lines of evidence suggest that p27^{Kip1} mediates G1 arrest induced by transforming growth factor β (TGFβ), contact inhibition, or serum deprivation in epithelial cell lines (Polyak et al., 1994a). TGFβ elevates the expression of the CDK4/CDK6-specific inhibitor p15^{Ink4B} and induces the release of p27^{Kip1} from CDK4 and CDK6. In turn, the released p27^{Kip1} apparently binds to the cyclin E–CDK2 complex, resulting in inhibition of its kinase activity (Reynisdóttir et al., 1995). In T cells, p27^{Kip1} is expressed at very high levels (Firpo et al., 1994; Nourse et al., 1994; this study). Moreover, it was recently shown that interleukin-2 (IL-2) eliminates p27^{Kip1} from T cells, thus leading to progression of the cell cycle from quiescence to the S phase (Nourse et al., 1994). The elimination of p27^{Kip1} by IL-2 is prevented by rapamycin. This implies that p27^{Kip1} may act to hold T cells in a quiescent state (G0). These findings support the notion that p27^{Kip1} may play a central role in the negative regulation of cell growth in a broad range of tissues.

Gene targeting in embryonic stem (ES) cells provides

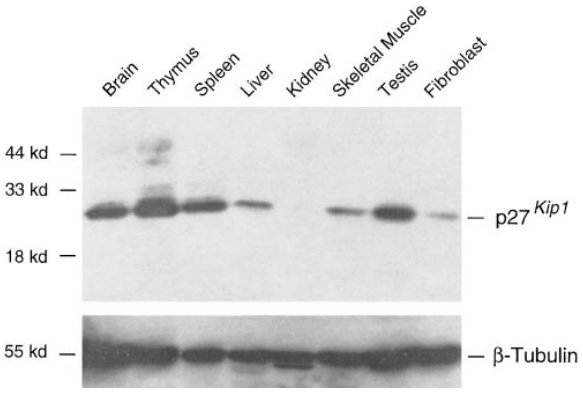

Figure 1. Immunoblot Analysis of p27^{Kip1} in Multiple Tissues

Expression of p27^{Kip1} was assessed by immunoblot analysis with an anti-p27^{Kip1} MAb. Lysates from the indicated organs (50 μg of protein equivalent) were loaded in each lane. The amount of protein and the integrity of transfer were verified by staining with Ponceau-S solution (Sigma). As a control, expression of β-tubulin was also assessed with an anti-β-tubulin antibody. Bands corresponding to p27^{Kip1} and β-tubulin are indicated.

a powerful tool for the disruption of a gene and generates a loss of function animal model (Mansour et al., 1988). While biochemical data implicate the involvement of p27^{Kip1} in the basic machinery controlling both cell growth and cell differentiation, we wanted to explore the biological importance of p27^{Kip1} in mouse development by this gene-targeting technology. Here we describe p27^{Kip1}-deficient animals displaying a variety of abnormalities. These data indicate that p27^{Kip1} acts to regulate the growth of multiple types of cells. The biological roles of p27^{Kip1} and a possible genetic link among pRb, cyclin D, and p27^{Kip1} are discussed.

Results

Tissue-Specific Expression of p27^{Kip1} Protein

The p27^{Kip1} mRNA is present at similar levels in various tissues (Polyak et al., 1994b). Since levels of p27^{Kip1} protein appear to be controlled mainly at the level of protein degradation by the ubiquitin/proteasome pathway (Pagano et al., 1995), we examined the protein expression of p27^{Kip1} in various murine tissues. Immunoblot analysis showed that p27^{Kip1} is highly expressed in thymus, spleen, brain, and testis, but there were relatively low levels in liver, kidney, skeletal muscle, and fibroblasts (Figure 1). This pattern of p27^{Kip1} expression correlates roughly with the sites of abnormalities that appeared in p27^{Kip1} gene–ablated mice, as described below.

p27^{Kip1} Gene Targeting

The murine p27^{Kip1} genomic locus comprises three exons spanning about 4 kb. The protein-coding region resides only in exons 1 and 2. Because these exons were contained within a 1.3 kb stretch of genomic DNA, the targeting construct was designed to delete the entire protein-coding region of the p27^{Kip1} gene (Figure 2A). Electroporation of the linearized targeting vector and G418/gancyclovir selection for homologous recombinants were carried out as described in Experimental Procedures. G418/gancyclovir double-resistant ES cell clones (160) were screened for homologous recombination events by the polymerase chain reaction, and 24 clones (15%) were found to be homologously recombined. All of these clones were confirmed to contain the desired targeted allele by Southern blot analysis (data not shown). Of these, 14 clones were injected into C57BL/6 blastocysts, and high coat color chimeric males that transmitted the mutant allele to the germline were obtained. Heterozygous offspring of chimeras appeared entirely normal and were fertile. Heterozygotes were bred to produce p27$^{-/-}$ mice, which were identified by Southern blot analysis of tail DNA (Figure 2B).

Tissues from p27$^{+/+}$, p27$^{+/-}$, and p27$^{-/-}$ animals were analyzed by immunoblot to determine the presence or absence of p27^{Kip1} protein (Figure 2C). Whole-cell lysates from the thymus at 4 weeks of age showed detectable amounts of p27^{Kip1} protein in p27$^{+/+}$ and p27$^{+/-}$ animals, but not in p27$^{-/-}$ animals. Of particular interest, the level of p27^{Kip1} protein was lower in p27$^{+/-}$ than in p27$^{+/+}$ mice, indicating a dose-dependent expression of the p27^{Kip1} alleles. In contrast, the amount of CDK2 was not altered in p27$^{-/-}$ thymocytes. However, CDK2 kinase activity was elevated in p27$^{-/-}$ thymocytes by approximately 10-fold in comparison with p27$^{+/+}$ or p27$^{+/-}$ cells (Figure 2D). Even though there was somewhat more p27^{Kip1} in the p27$^{+/+}$ than in the p27$^{+/-}$ thymocytes, CDK2 kinase activity was essentially the same. This represents direct genetic evidence indicating that a CDK inhibitor significantly suppresses the kinase activity of a CDK under physiological conditions.

Phenotype of p27$^{-/-}$ Mice

Heterozygote matings yielded wild-type (+/+), heterozygous (+/−), and nullizygous (−/−) offspring at roughly the expected Mendelian ratio, indicating no significant embryonic lethality. At birth, these homozygotes were indistinguishable from their wild-type and heterozygous littermates. Surprisingly, however, by 4–6 weeks of age it became evident that many, but not all, p27$^{-/-}$ mice weighed more than the littermate control animals (Figures 3A and 3B). This weight difference became more pronounced with age. In most cases, they were the largest animals in an individual litter, although some of the mutant animals did not gain weight any faster than the control animals. The reason for this heterogeneity in phenotype is uncertain, but is probably due to the mixed genetic background (129/Ola and C57BL/6) of the mice.

Despite the increased body size of the p27$^{-/-}$ mice, the outward appearance of these mice showed normal proportions (Figure 3A). The only exception was a significantly swollen scrotum in adult male p27$^{-/-}$ mice (data not shown; see Figure 6). This increased body weight was not due to simple obesity, because the weight of all organs tested had increased in proportion to the whole body weight except for several enlarged organs, including the thymus, spleen, testis, ovary, pituitary gland, adrenal gland, and prostate, as described below. The levels of growth hormone in serum from p27$^{-/-}$ mice were comparable with those from littermate controls (data not shown). There was no evidence of illness in the p27$^{-/-}$ mice up to 7 months of age, suggesting that

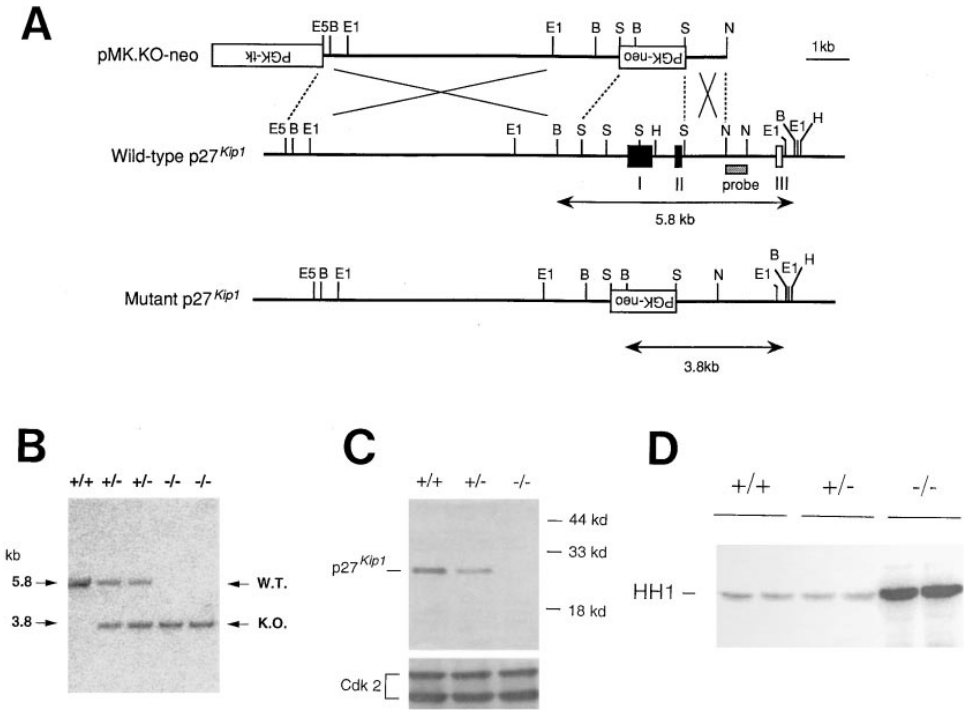

Figure 2. Targeted Disruption of the Mouse p27Kip1 Gene

(A) Structure of the targeting vector, pMK.KO–neo, restriction map of the mouse p27Kip1 gene, and the structure of the mutated locus following the homologous recombination. The coding exons are depicted by closed boxes and are numbered; the open box denotes the noncoding portion of the third exon. The structure of the noncoding portion of the first exon has not been determined. A genomic fragment used as a probe for Southern blotting is shown as a stippled box. Abbreviations are as follows: PGK–neo, the neomycin transferase gene linked to the phosphoglycerate kinase (PGK) promoter; PGK–tk, thymidine kinase gene derived from herpes simplex virus linked to the PGK promoter. Both PGK–neo and PGK–tk were placed in a reverse orientation relative to the p27Kip1 transcription. Restriction site abbreviations: B, BamHI; E1, EcoRI; E5, EcoRV; H, HindIII; N, NdeI; S, SmaI. Portions of all NdeI sites have not been fully determined. Expected sizes of the BamHI fragments that hybridize with the probe are indicated.

(B) Southern blot analysis of genomic DNA extracted from mouse tails. The DNA was digested with BamHI and hybridized with the probe. The sizes of wild-type (W.T.) and disrupted (K.O.) alleles are shown; the genotypes of mice are presented above the lanes.

(C) Immunoblot analysis of extracts prepared from $p27^{+/+}$, $p27^{+/-}$, and $p27^{-/-}$ mouse thymocytes. Whole-cell lysates of thymocytes derived from the indicated mouse genotypes were subjected to SDS–PAGE and blotted to the membrane. The blot was probed with anti-p27Kip1 MAb and then reprobed with rabbit anti-CDK2 antibody. Bands corresponding to p27Kip1 and CDK2 are indicated. CDK2 mRNA in mouse cells is translated as two protein isoforms of 32 and 40 kDa (Noguchi et al., 1993).

(D) CDK2 kinase assay in vitro. Whole-cell lysates of thymocytes derived from six independent mice with the indicated genotypes were immunoprecipitated with anti-CDK2 antibody plus protein A–agarose beads and then subjected to in vitro kinase assay. Bands corresponding to histone H1 are indicated. Quantitation by a BAS 3000 image analyzer indicates that the average intensity of the bands is 100 (+/+), 88 (+/−), and 998 (−/−).

the absence of p27Kip1 does not increase the occurrence rate of cancer except for pituitary tumors described below.

Lack of p27Kip1 Results in a Strikingly Enlarged Thymus

At necropsy, thymi from $p27^{-/-}$ mice were found to be grossly enlarged (Figure 4A); they sometimes totally covered the heart. The number of thymocytes contained in the enlarged thymus was so elevated that it sometimes reached 1×10^9 cells per thymus at 4 weeks of age (Figure 4B). Nevertheless, flow cytometric analysis showed that the CD4/CD8 and αβ T cell receptor (TCR) profiles of the thymocytes from the mutant animals were always within a normal range (Figure 4C). Histopathological examination of thymi from mice lacking p27Kip1 revealed relatively normal architecture in spite of the extreme increase in size (Figure 4D). These data indicate that all populations of thymocytes expand proportionally and that lymphoid malignancy is unlikely to account for the swelling of the thymus. The percentage of cycling cells in the thymus from $p27^{-/-}$ mice was comparable with that from control mice (data not shown). However, because the total cell number was increased, the absolute number of cycling cells was also augmented in the thymus, suggesting that the cycling ancestor cells may increase and produce descendants resulting in the expansion of all populations of thymocytes.

Since it has been believed that about 97% of thymocytes die in the thymus during selection (Egerton et al., 1990), a lower sensitivity to apoptosis of thymocytes from the $p27^{-/-}$ mice might be responsible for the enlargement. However, we could not find a marked difference among thymocytes from $p27^{+/+}$, $p27^{+/-}$, and $p27^{-/-}$ mice in culture with respect to susceptibility to spontaneous apoptosis, γ-irradiation-induced apoptosis, or

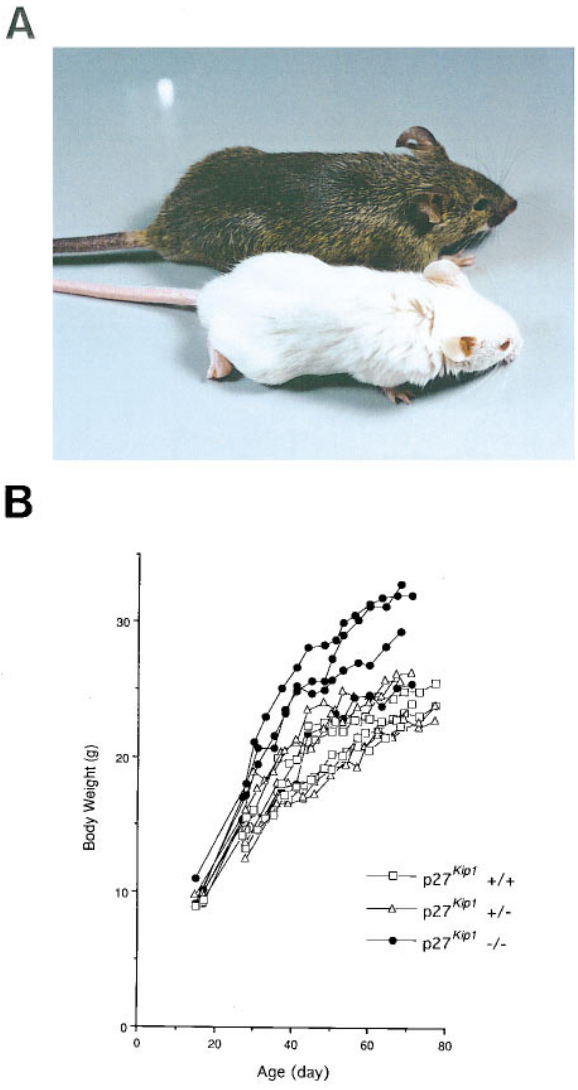

Figure 3. Appearance of $p27^{-/-}$ Mice

(A) Larger body in $p27^{-/-}$ mice. The agouti mouse is a $p27^{-/-}$ mice; the white mouse is wild type. Both mice were 12-week-old littermates. Note that the enlargement of the body seems to be proportional rather than obese.

(B) Representative growth curve of wild-type (open squares), heterozygous (open triangles), and $p27^{-/-}$ (closed circles) littermates, as indicated in the figure. Mice were weighed at intervals and plotted against age in days.

dexamethasone-induced apoptosis (data not shown). We also examined the blood level of corticosterone, which affects size of thymus by controlling apoptosis of thymocytes. No obvious alteration in corticosterone levels was observed in $p27^{-/-}$ mice (data not shown). Histological examination of the adrenal gland showed marked hyperplasia of the medulla in $p27^{-/-}$ mice, whereas the cortex remained relatively normal (data not shown).

Compared with the dramatic abnormality in the thymus, changes in peripheral lymphoid organs were less striking. Some mice with larger body sizes contained more T cells in their spleens and lymph nodes by up to 2-fold. In contrast, the number of B cells found in spleens, lymph nodes, and bone marrow from these mice was normal: no abnormality could be observed in B cell development by flow cytometric analysis (data not shown). Almost all lymphocytes in the spleen and lymph nodes from the mutant mice remained in the G0 phase, indicating that $p27^{Kip1}$ is not essential for maintaining quiescence of peripheral lymphocytes. However, lack of $p27^{Kip1}$ may retard the timing of the exit from the cell cycle, result in more cell cycles during the early development of T cells in the thymus, or both.

TGFβ and Rapamycin Inhibit the Proliferation of $p27^{-/-}$ T Cells

It was recently shown that IL-2 treatment results in the elimination of $p27^{Kip1}$ from peripheral T cells (Nourse et al., 1994). This raised the possibility that $p27^{Kip1}$ may regulate the timing of onset or the amplitude of proliferation upon stimulation (or both). T cells from the lymph nodes of $p27^{+/+}$, $p27^{+/-}$, and $p27^{-/-}$ mice were prepared, and proliferation was tested with anti-CD3 and anti-CD28 monoclonal antibodies (MAbs) in the presence or absence of IL-2. Unexpectedly, the proliferation of $p27^{-/-}$ T cells upon mitogenic stimulation was comparable with that of the $p27^{+/+}$ or $p27^{+/-}$ T cells (Figure 5). IL-2 augmented the response to anti-CD3 plus anti-CD28 MAbs of T cells, and there was no significant difference in this augmentation among $p27^{+/+}$, $p27^{+/-}$, and $p27^{-/-}$ T cells (data not shown).

It has been generally accepted that $p27^{Kip1}$ mediates the cell cycle–inhibitory signal of TGFβ. Since TGFβ is known to be a potent inhibitor of lymphocyte proliferation (Kehrl et al., 1986; Ahuja et al., 1993), the effect of TGFβ on $p27^{Kip1}$-deficient lymphocytes was tested. Surprisingly, TGFβ clearly inhibited the growth of $p27^{-/-}$ T cells as well as that of the $p27^{+/+}$ and $p27^{+/-}$ T cells (Figure 5). Thus, we conclude that $p27^{Kip1}$ is not essential for the inhibitory effect of TGFβ on the cell cycle. We next sought to examine the effect of the anti-proliferative compound, rapamycin, which prevents IL-2-induced elimination of $p27^{Kip1}$ (Nourse et al., 1994). Upon stimulation, rapamycin treatment inhibited the proliferation of T cells from $p27^{+/+}$, $p27^{+/-}$, and $p27^{-/-}$ mice in a similar dose-dependent manner (Figure 5). This indicates that the inhibitory effect of rapamycin on T cell growth does not require $p27^{Kip1}$.

$p27^{-/-}$ Mice Demonstrate Testicular and Ovarian Hyperplasia

Enlargement of testis was anticipated before necropsy because of the high expression level of $p27^{Kip1}$ in testis and the extremely protruded scrotum in adult male mice lacking $p27^{Kip1}$. Macroscopic examinations indicated that testis and ovary were about 2-fold larger in $p27^{-/-}$ mice than in $p27^{+/+}$ or $p27^{+/-}$ mice (Figures 6A and 6B). Histopathological examination did not show obvious structural abnormalities in testis except for the remarkable hyperplasia (data not shown). In agreement, male $p27^{Kip1}$ gene–disrupted mice were fertile, indicating normal development and function of spermatids in testis.

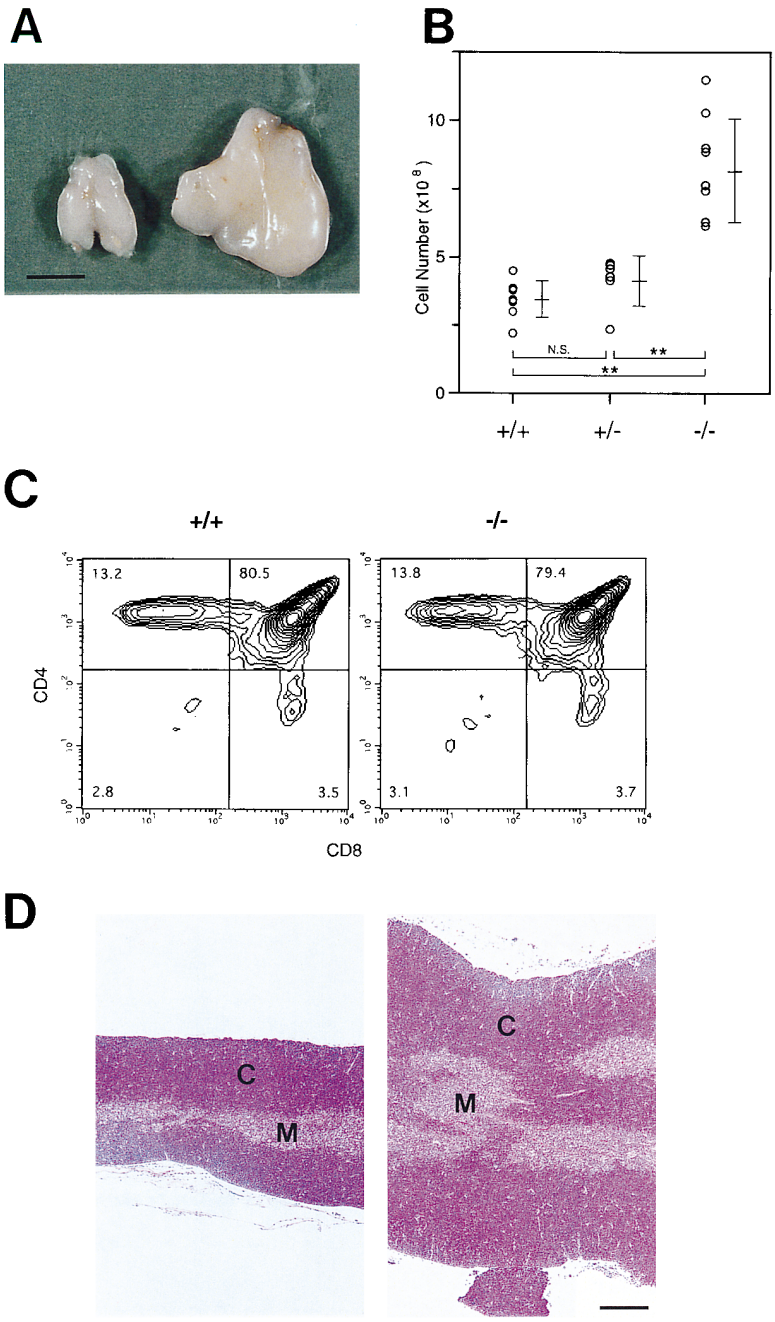

Figure 4. Extensive Hyperplasia in p27$^{-/-}$ Thymus

(A) Gross appearance of thymi from a wild-type mouse (left) and a p27$^{-/-}$ mouse (right). The thymus from the mutant mouse seems to be proportionally enlarged. Scale bar is 5 mm.

(B) Total cell numbers contained in whole thymi from 4-week-old p27$^{+/+}$, p27$^{+/-}$, and p27$^{-/-}$ mice. The mean and standard deviations are shown. Statistical analysis was done with a two independent sample t test. Two-tailed P values are <0.01 (double asterisks). NS, not significant.

(C) Flow cytometric analysis of thymocytes from a 4-week-old wild-type mouse (left) and a p27$^{-/-}$ mouse (right). No significant differences were observed.

(D) Histopathological sections of thymi derived from a 4-week-old wild-type mouse (left) and a 4-week-old p27$^{-/-}$ mouse (right). The paraffin sections were stained with hematoxylin and eosin. The p27$^{-/-}$ thymus retains a relatively normal ratio of cortex (C) and medulla (M), but contains a large number of thymocytes. Scale bar is 200 μm.

Thus far, we have failed to detect pregnancy in female p27$^{-/-}$ mice, indicating that female mutant mice are sterile. In ovaries from the 4-week-old female p27$^{-/-}$ animals, a marked accumulation of atypical follicles with extensive hyperplasia of granulosa cells was observed, whereas theca cells around the follicles seemed to remain normal (Figures 6C and 6D). The endometrium and interstitial tissue of the uterus were always hyperplastic, suggesting a high production of estrogen from the hyperplastic ovarian follicles (data not shown). In the atypical follicles, the formation of the cavity (antrum) was much less prominent than that seen in normal mice. Indeed, Graafian follicles were not evident in ovaries from p27$^{-/-}$ mice. These follicles also contained fewer apoptotic cells and degenerative granulosa cells, which were commonly seen in atretic follicles of normal mice. Moreover, the formation of the corpus luteum was not observed in 12-week-old p27$^{-/-}$ mice, whereas it was readily found in ovaries from age-matched control animals (Figures 6E and 6F). Consequently, the ovarian follicles from the p27$^{-/-}$ mice appeared to be homogeneous. Most of the accumulated follicles were primary and secondary follicles, but further development appeared to be impaired. In contrast, ovaries from normal animals displayed a variety of developmental stages, containing primary follicles, secondary follicles, Graa-

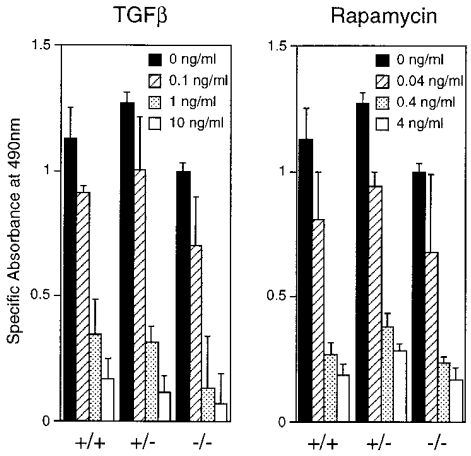

Figure 5. Inhibition of T Cell Proliferation by TGFβ or Rapamycin

Inhibitory effects of TGFβ (left) and rapamycin (right) on T cell proliferation with immobilized anti-CD3 and anti-CD28. TGFβ and rapamycin were added in culture at the indicated concentrations. Shown are the mean ± standard deviations of specific absorbance at 490 nm from triplicated cultures. Specific absorbance means values from which background (absorbance without stimulations) was reduced. Genotypes of T cells are shown at the bottom of the figure.

fian follicles, atretic follicles, and corpus luteum. These histological findings suggest an impairment of ovulation from p27$^{-/-}$ ovaries.

High Incidence of Pituitary Tumors in p27$^{-/-}$ Mice

Mice heterozygous for the *Rb* mutation, or chimeric for homozygous inactivation of *Rb*, are highly predisposed to intermediate lobe pituitary tumors (Jacks et al., 1992; Lee et al., 1992; Williams et al., 1994). Given the biochemical connection between pRb and p27^{Kip1}, we focused on pathological examinations of the pituitary gland in p27$^{-/-}$ mice. The pituitary gland was usually hyperplastic in p27$^{-/-}$ mice. At 4 weeks of age, the weight of the pituitary was more than 2-fold that of the wild-type pituitary (data not shown). Histopathological examination revealed that the intermediate lobes, a vestigial structure in adult humans, were hyperplastic, while the anterior and posterior lobes maintained relatively normal architecture. About half of p27$^{-/-}$ mice were found to develop a pituitary tumor, originating from the intermediate lobe, by 12 weeks of age (Figure 7A). There was a large number of atypical cells in the intermediate lobe that showed an irregularly shaped nucleus with an increased content of chromatin and pleomorphism in size. Also, the cellular sheets displayed irregularly increased thickness and papillary protrusion, which suggested proliferation beyond a regenerative or hyperplastic nature. The atypical cells tended to form a cystic structure (Figure 7C). Hemorrhage was often seen in the cysts, sometimes leading to the formation of a large hematoma. Based on these morphological features, we diagnosed the lesion as "benign pituitary adenoma." This pituitary tumor showed no sign of invasion or metastasis

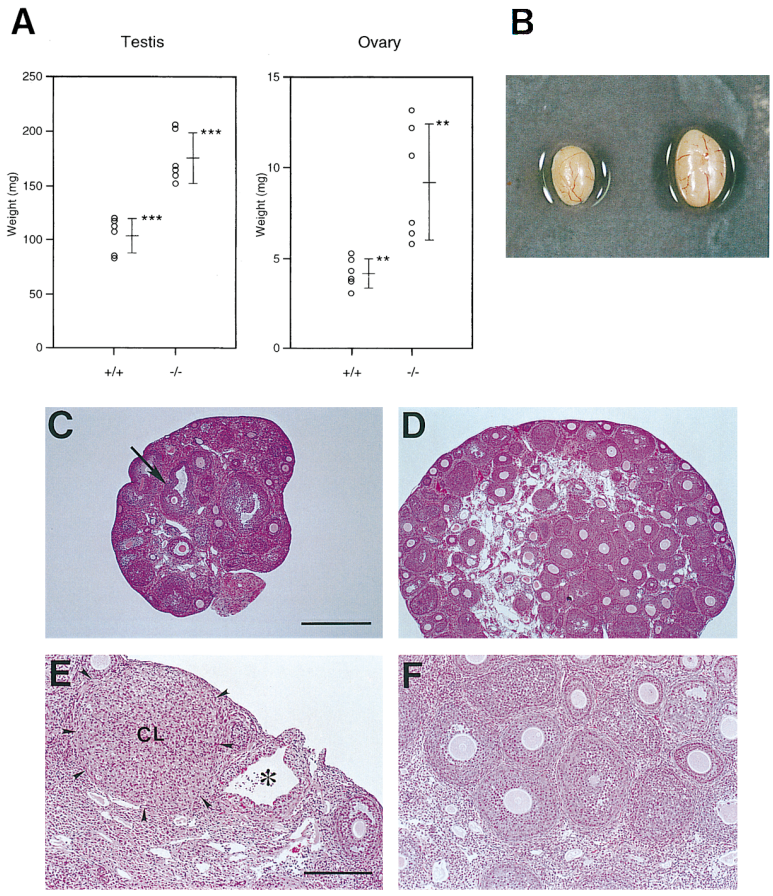

Figure 6. Testicular and Ovarian Hyperplasia in p27$^{-/-}$ Mice

(A) Weight of testes (left) and ovaries (right) from 12-week-old p27$^{+/+}$ and p27$^{-/-}$ mice. The mean and standard deviations are shown. Statistical analysis was done with a two independent sample t test. Two-tailed P values are <0.01 (double asterisks) or <0.001 (triple asterisks).

(B) Gross appearance of testes from a wild-type mouse (left) and a p27$^{-/-}$ mouse (right).

(C–F) Histopathological sections of ovaries derived from 4-week-old (C and D) or 12-week-old (E and F) wild-type (C and E) or p27$^{-/-}$ mice (D and F). The paraffin sections were stained with hematoxylin and eosin. Atypical ovarian follicles with remarkable hyperplasia of granulosa cells are accumulated in the p27$^{-/-}$ ovary. Arrow in (C) indicates a Graafian follicle; arrowheads in (E) indicate corpus luteum (CL); the asterisk (E) marks a follicle just after ovulation. Scale bar is 500 μm in (C) and (D) and 200 μm in (E) and (F).

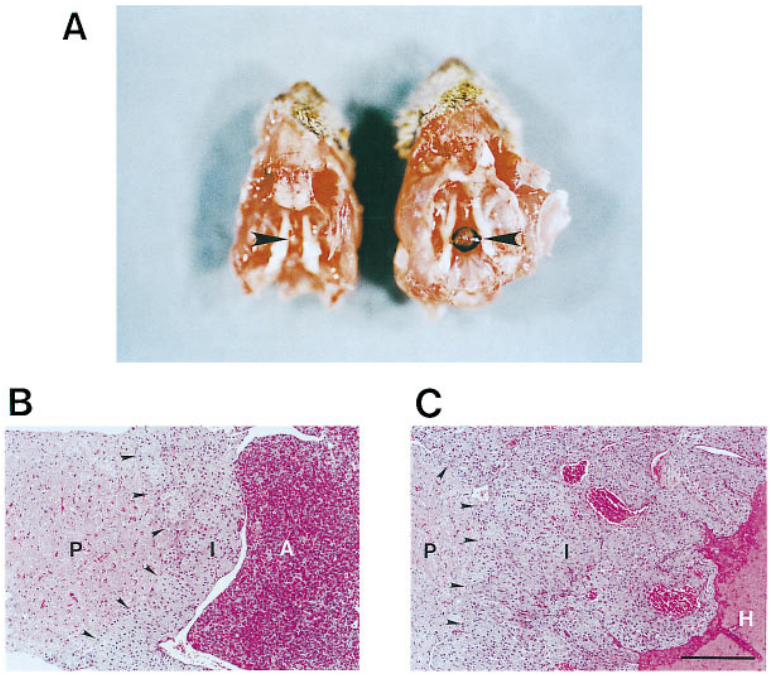

Figure 7. Spontaneous Pituitary Tumor in p27$^{-/-}$ Mice

(A) Macroscopic appearance of a pituitary tumor that had developed in a 12-week-old p27$^{-/-}$ mouse (right). A wild-type littermate is also shown (left). Arrowheads indicate pituitary glands.

Histopathological sections of pituitary glands are shown in (B) and (C).

(B) Normal pituitary gland from a 12-week-old wild-type mouse. P, posterior lobe; I, intermediate lobe; A, anterior lobe. Arrowheads indicate the boundary between posterior and intermediate lobes.

(C) The pituitary tumor that had developed in a 12-week-old p27$^{-/-}$ mouse. Note that the intermediate lobe is extremely hyperplastic with an irregular margin and that several cysts filled with blood had formed. H, a portion of large hematoma. The anterior lobe is not seen in this picture. Scale bar is 100 μm.

in mice up to 7 months of age. Long-term observation will be necessary to gauge the late-onset lethality of this tumor in p27$^{-/-}$ mice.

Disorganized Layer Pattern in Retina

Histopathological examination of the retinas of p27^{Kip1}-deficient mice showed a marked disorganization of the cellular layer pattern in the neural retina. The outer granular layer, which is composed of the nuclei of photoreceptor cells, invaded the layer of rods and cones beyond the outer limiting membrane (Figure 8A). The lesion was not diffuse but was scattered. The degree of severity varied, probably owing to the mixed genetic background of the mice. The outer limiting membrane was irregular and not clearly recognizable in some regions. In addition, in the inner granular layer, a displacement of bipolar cells, with an increase in the number of amacrine cells (astrocyte-like cells) and Muller's supporting cells, and a disorganization of the network of cell fibers were also observed. The pigment epithelium layer was thickened, and cells composing the pigment epithelium were taller than normal. The lack of a secondary response, such as phagocytosis of the abnormal photoreceptor cells by pigment epithelial cells, indicates that the abnormality of photoreceptors may be developmental.

To elucidate the cause of the highly focused abnormality seen in the neural retina of p27$^{-/-}$ mice, we examined the pattern of p27^{Kip1} protein expression in the retina of normal mice using an immunohistochemical approach. Specific expression of the p27^{Kip1} protein could be exclusively detected in the photoreceptor cells (Figure 8B). This intense expression of p27^{Kip1} in photoreceptors in wild-type mice may explain the profound effect of p27^{Kip1} inactivation on the outer layers of the retina. The slight disorganization seen in the inner granular layer and the pigment epithelium layer of p27$^{-/-}$ mice might be attributable either to a secondary effect related to the abnormality of the photoreceptor cells or to a low expression of p27^{Kip1}, undetectable by our immunohistochemisty.

To determine whether retinas of the mutant mice were able to respond properly to light, we measured electrophysiologic potentials generated in the retina following exposure of the mice to a short pulse of light. Two waves of electrical signaling can be observed in this electroretinographic (ERG) study: the a wave arises mainly from the photoreceptors, while the b wave is generated largely by bipolar cells. We carried out ERG studies with p27$^{-/-}$ mice soon before necropsy, and compared the ERG results with the histopathological findings. Severely affected p27$^{-/-}$ mice showed an approximately 2-fold reduction of their ERG amplitudes (Figure 8C), while mildly or moderately affected mice usually showed an almost normal ERG pattern. The observed reduction in ERG amplitudes could be accounted for by the partial loss of the rod and cone layer.

p27^{Kip1} Is Not Required for the G1 Arrest in Embryonic Fibroblasts

Mouse embryonic fibroblasts (MEFs) were prepared from p27$^{+/+}$ and p27$^{-/-}$ 13.5 days postcoitum (dpc) embryos, and the initial growth properties of these MEFs during culture in vitro were examined. At passage 3, all of the MEFs, irrespective of their genotype, grew quite rapidly and had similar growth rates before reaching confluence (Figure 9A). All MEFs showed contact inhibition, and there was no significant difference in saturation densities between p27$^{+/+}$ and p27$^{-/-}$ MEFs. At passage 6, the growth of both p27$^{+/+}$ and p27$^{-/-}$ MEFs slowed, and we could not observe any significant difference in saturation densities between p27$^{+/+}$ and p27$^{-/-}$ MEFs (data not shown).

G1 arrest in MEFs is induced in response to many extracellular signals, including contact inhibition, serum

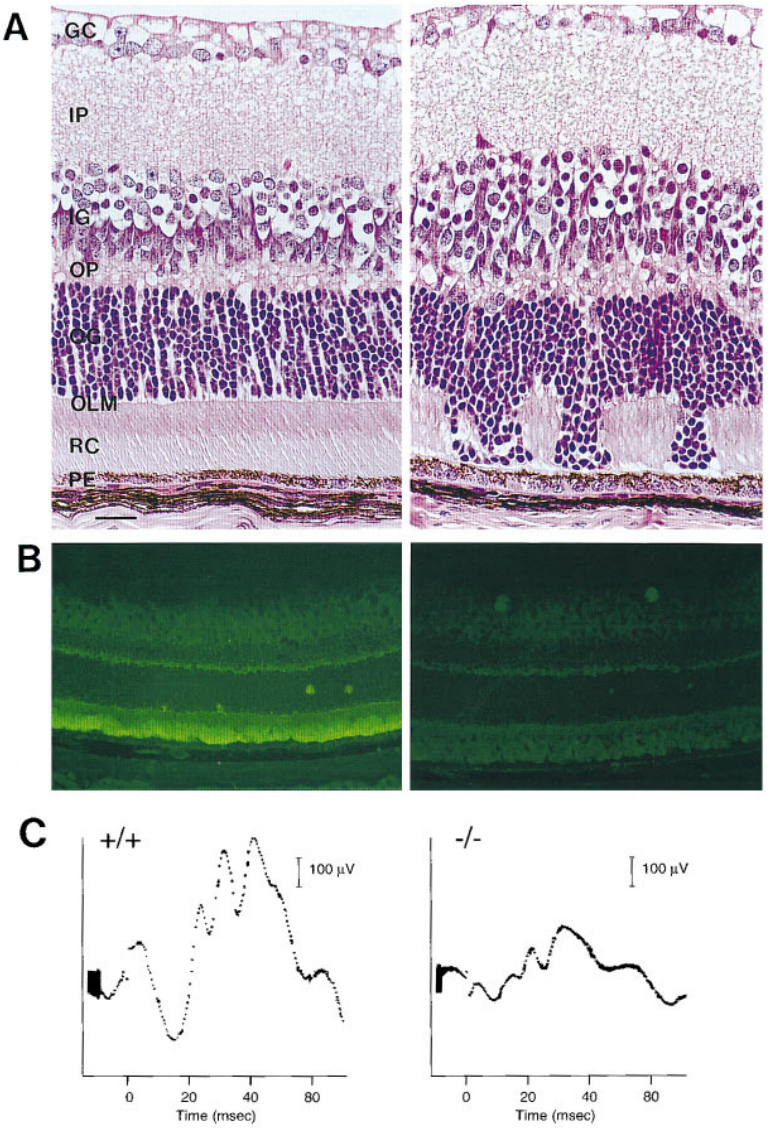

Figure 8. Disorganized Retinal Layers in p27$^{-/-}$ Mice

(A) Histological sections of retinas derived from 4-week-old p27$^{+/+}$ (left) and p27$^{-/-}$ mice (right). The paraffin sections were stained with hematoxylin and eosin. Abbreviations are as follows: GC, ganglion cell layer; IP, inner plexiform layer; IG, inner granular layer; OP, outer plexiform layer; OG, outer granular layer; OLM, outer limiting membrane; RC, rods and cones layer; PE, pigment epithelium. Scale bar is 20 μm.

(B) Immunohistochemical examinations for p27^{Kip1} expression in a wild-type mouse. Cryostat sections were incubated with anti-mouse p27^{Kip1} MAb followed by anti–mouse IgG1 antibody conjugated with FITC (left) or only with secondary antibody (right). Specific expression of p27^{Kip1} is seen exclusively in the photoreceptor cells.

(C) Representative ERG potentials recorded from a 12-week-old wild-type (left) and a p27$^{-/-}$ (right) mouse in response to a 0.3 joule Xenon light delivered at time 0.

starvation, DNA damage due to γ-irradiation, and metabolic perturbations by chemicals such as N-phosphonacetyl-L-aspartate (PALA), which is a specific inhibitor of de novo uridine biosynthesis (Swyryd et al., 1974). We tested p27$^{-/-}$ MEFs as to whether G1 arrest caused by these treatments was maintained. However, we could not find any significant increase in S phase (or decrease in G1 phase) of p27$^{-/-}$ MEFs compared with wild-type MEFs in response to contact inhibition, serum starvation, γ-irradiation, or PALA treatment (Figures 9B and 9C). Thus, it appears that the G1 arrest caused by these treatments does not require p27^{Kip1}.

Discussion

The biological roles of the CDK inhibitors are largely unknown, although extensive studies have emerged concerning the putative roles of CDK inhibitors in cell cycle control, cancer, and development (reviewed by Sherr and Roberts, 1995). Despite specific expression of p21^{Cip1} in cells or tissues undergoing differentiation, mice lacking p21^{Cip1} exhibit neither developmental abnormalities nor early tumorigenesis. In contrast, the studies concerning the p27^{Kip1} gene–ablated mice presented here have both refined and broadened the roles for p27^{Kip1}. Because p27^{Kip1} has been considered as a mediator of contact inhibition, we anticipated that homozygous inactivation of the p27^{Kip1} gene in the mouse germline would severely compromise tissue organization in the developing embryo, leading in turn to early embryonic lethality. However, p27$^{-/-}$ mice complete an apparently normal prenatal development and are born at roughly the expected Mendelian ratio.

Increased Body Size

An apparent phenotype observed in the p27$^{-/-}$ mice was that the mice were significantly larger in size than control littermates. This increase of body size was found to be of late onset: it started at about 4–6 weeks postnatally. This is consistent with the fact that the expression level

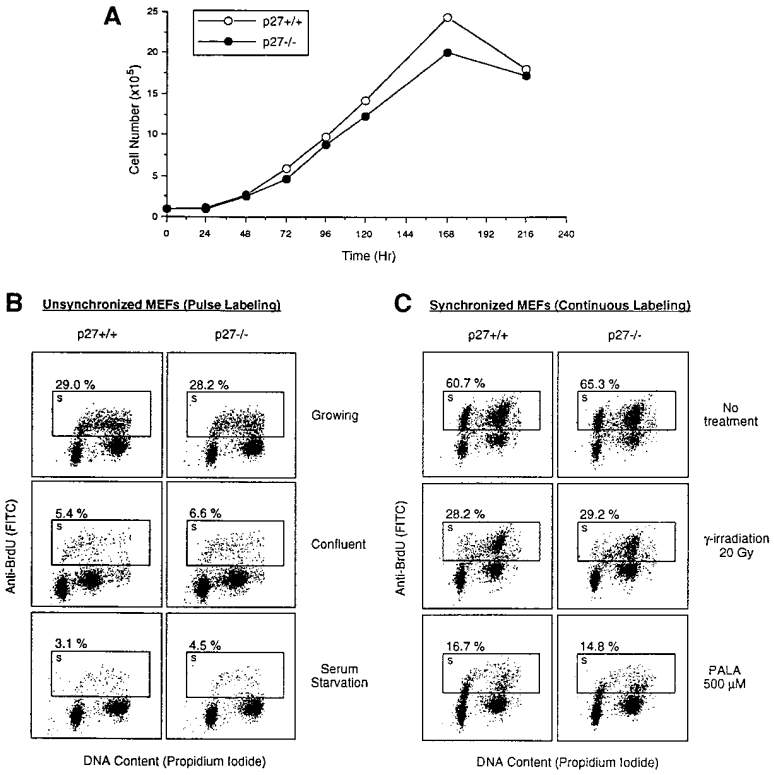

Figure 9. Growth Properties and G1 Arrest in MEFs Remain Normal in p27$^{-/-}$ Mice

(A) Saturation densities and growth analyses of MEFs derived from p27$^{+/+}$ (open circles) and p27$^{-/-}$ (closed circles) mice at passage 3. Cells (10^5) were plated in 100 mm culture dishes as described in Experimental Procedures. Cell number at each timepoint represents the average of duplicate plates.

(B and C) The ability to block S phase entry in p27$^{+/+}$ and p27$^{-/-}$ MEFs. Representative two-color flow cytometric analyses of unsynchronized (B) or synchronized (C) p27$^{+/+}$ and p27$^{-/-}$ MEFs are shown with the percentage of cells entering S phase (BrdU$^+$, boxed) after the indicated treatments.

(B) MEFs were harvested at logarithmic growth (top), after reaching confluence (middle), or after a 48 hr culture in serum-starved media (bottom) with 10 μM BrdU labeling for 30 min prior to harvest. Cells were stained for DNA content with propidium iodide and for replicative DNA synthesis with anti-BrdU antibody conjugated with FITC. (C) Serum-starved cells were released into complete media containing 10 μM BrdU with no treatment (top), with 20 Gy γ-irradiation (middle), or with 500 μM PALA (bottom). At 24 hr after release, cells were harvested and stained.

of p27^{Kip1} in day-10 embryos seems to be barely detectable (Toyoshima and Hunter, 1994). Although it has been believed that contact inhibition may play an important role in development, the molecular basis of contact inhibition remains largely unclear. While the hypothesis that a CDK inhibitor, p27^{Kip1}, may mediate growth suppression when cells become confluent is fascinating, we demonstrated that p27$^{-/-}$ MEFs retained the property of contact inhibition in vitro. However, it is possible that there may be several types of contact inhibition and that one of them that requires p27^{Kip1} for growth suppression might be responsible for controlling the size of organs at a later phase of development. Such a type of contact inhibition may play a role as a "brake" on growth, which might not be required during embryogenesis because of the extensive growth rate of the embryo.

We have compared the percentage of proliferative cell nuclear antigen–positive cells as cycling cells in mutant and control animals by immunohistochemistry, and we could not detect any significant difference (data not shown). However, because the size of the organs was enlarged, the absolute number of cycling cells increased as the total cell number increased. This may have resulted in the larger body size of the mutant animals.

Tumor Suppressive Activity of p27^{Kip1}

Recently, evidence is accumulating that many molecules involved in oncogenesis are also involved in cell cycle control. An oncosuppressor gene, *Rb*, negatively regulates the cell cycle and is probably regulated by the cyclin D–CDK4 kinase complex. Mutations of *Rb* lead to retinoblastoma in humans, whereas mice heterozygous for a mutant *Rb* allele develop pituitary tumors by 1 year of age (Jacks et al., 1992; Lee et al., 1992; Williams et al., 1994). In addition, cyclin D1 is amplified in a subset of human cancers, acting as an activated oncogene (Motokura et al., 1991; Lammie et al., 1991; Gillett et al., 1994). By regulating cyclin–CDK complex activity, individual CDK inhibitors are potential tumor suppressors. Indeed, mutations or deletions in the human p16/p15 locus are common in esophageal carcinomas and melanomas (Mori et al., 1994; Hussussian et al., 1994). However, there has not been direct evidence indicating that other CDK inhibitors act as oncosuppressors.

In humans, the p27^{Kip1} gene was mapped to the short arm of chromosome 12 at the 12p12–12p13.1 boundary (Ponce-Castaneda et al., 1995), which is reported to harbor deletions and rearrangements in leukemias and mesotheliomas (Chan et al., 1992; Decker et al., 1990). Despite an extensive search for molecular aberrations modifying the human p27^{Kip1} locus, no significant alterations of the p27^{Kip1} gene have been reported (Bullrich et al., 1995; Pietenpol et al., 1995; Ponce-Castaneda et al., 1995; Kawamata et al., 1995; Morosetti et al., 1995). Heterozygous *Rb*$^{+/-}$ mice acquire *Rb*$^{-/-}$ tumors later in life, originating from the intermediate lobe of pituitary gland (Jacks et al., 1992; Lee et al., 1992; Williams et al., 1994). Similar pituitary tumors arise in the p27$^{-/-}$ mice. Although the phenotype of p27 mutant mice was less severe than that of *Rb* mutant mice, this similarity may reflect some common underlying molecular process responsible for regulating pituitary cell proliferation and differentiation. Future examinations might reveal a genetic aberration in the p27^{Kip1} locus in human pituitary tumors. Given that p27^{Kip1} inhibits the cyclin D–CDK4 kinase complex, which phosphorylates pRb leading to

its inactivation, one would speculate that loss of $p27^{Kip1}$ might result in constitutive inactivation of pRb owing to hyperphosphorylation. The phosphorylation state of pRb in $p27^{-/-}$ cells will be tested. It is noteworthy that $p27^{-/-}$ animals display hyperplasia of the adrenal medulla, which is also observed in mice chimeric for homozygous inactivation of *Rb* (Williams et al., 1994).

Multiple Organ Hyperplasia

There was tissue specificity with respect to the abundance of $p27^{Kip1}$ protein: lymphocytes, gonad cells, and neurons appeared to express $p27^{Kip1}$ highly, whereas liver, kidney, skeletal muscle, and fibroblasts had a relatively small amount of $p27^{Kip1}$. A common feature among the lymphoid, reproductive, and nervous systems is that progenitor cells are mitotic and cycling vigorously, but thereafter the cell cycle stops, leading to a postmitotic state in which many cells are destined to die by programmed cell death. Finally, the surviving cells become mature, but still remain in a quiescent (G0) stage. Consistent with the abundance of $p27^{Kip1}$ in these tissues, the major abnormalities that occurred in $p27^{Kip1}$ gene–ablated mice were enlargement of thymus, testis, ovary, and adrenal medulla and a possible overgrowth of the neuroepithelium in retina. The reason that the brain weight did not increase as strikingly as the thymus did was not clear, but it is possible that redundant molecules may exist. Alternatively, the skull may somehow limit the size of the brain, whereas the thymus and testis or ovary have room to expand in the thoracic and the peritoneal cavities, respectively.

Growth expansion of thymocytes normally begins at the CD4/CD8 double-negative stage and is mediated by a signal from an immature TCR complex comprised of pTα and TCRβ (Mombaerts et al., 1992; Fehling et al., 1995). This signal mediates not only growth but also differentiation to the CD4/CD8 double-positive stage. Thereafter, a cell stops cycling and becomes quiescent. We hypothesize that the period in which a cell is cycling may be longer in $p27^{-/-}$ thymocytes, probably due to a retardation of cell cycle arrest at the CD4/CD8 double-positive stage. Indeed, the absolute number of cells that were cycling was greater in the thymus of $p27^{-/-}$ mice (unpublished data). Redundant molecules, such as $p21^{Cip1}$, may finally act to pause the cell cycle in the thymus. Finer analyses will be necessary to prove this hypothesis.

Despite the marked hyperplasia in testis from $p27^{-/-}$ mice, $p27^{Kip1}$ is apparently not necessary for functional maturation of spermatids: male $p27^{-/-}$ mice were fertile. In contrast, female $p27^{-/-}$ mice apparently sterile. This is probably due to a maturation arrest of ovarian follicles. The block seems to reside in the formation of the cavity (antrum) in the follicles, because Graafian follicles were not found in $p27^{-/-}$ ovaries. We speculate that $p27^{Kip1}$ is responsible for the proper timing of the growth arrest of granulosa cells, which leads to the formation of cavity.

A Dispensable Role of $p27^{Kip1}$ in Signaling via TGFβ

Most studies concerning the anti-mitogenic activity of TGFβ have been performed using two epithelial cell lines, Mv1Lu mink lung epithelial cells and HaCaT human keratinocytes. A recent study by Reynisdóttir et al. (1995) demonstrated that TGFβ elevates expression of the CDK4/CDK6-specific inhibitor $p15^{Ink4B}$ and induces the release of $p27^{Kip1}$ from CDK4 and CDK6, which in turn is transferred to the cyclin E–CDK2 complex. We could not examine the anti-mitogenic activity of TGFβ in epithelial cells lacking $p27^{Kip1}$ because the establishment of a primary culture system with epithelial cells is in progress. TGFβ is also a potent immunoregulatory agent that inhibits lymphocyte proliferation. Both lymphocytes and monocytes produce TGFβ, suggesting a role for TGFβ in the host immune response (Kehrl et al., 1986; Wahl et al., 1989; Ahuja et al., 1993). In T cells, TGFβ also inhibits the phosphorylation of the pRb in response to mitogenic signals. Taken together, these results suggest that inhibition of T cell proliferation by TGFβ seemed to be, at least in part, mediated by $p27^{Kip1}$, which inactivates cyclin D and CDK4/CDK6 kinase complexes, leading to the prevention of pRb phosphorylation. Here, however, we demonstrate that $p27^{Kip1}$ was not essential for mediating anti-mitogenic signals via TGFβ in T cells. If the signaling pathway of TGFβ in T cells is identical to that in Mv1Lu and HaCaT cell lines, the surge in $p15^{Ink4B}$ levels induced by TGFβ would be sufficient to pause the cell cycle at the G1 phase. Mice lacking TGFβ display premature death due to severe autoimmune myocarditis (Shull et al., 1992), while $p27^{Kip1}$-deficient mice have never developed such autoimmune disorders. This genetic evidence further suggests that the pathways involving TGFβ and $p27^{Kip1}$ are not identical.

Retinal Development and Cell Cycle Control: A Genetic Link among pRb, Cyclin D, and $p27^{Kip1}$

Here we demonstrated that photoreceptor cells exclusively express $p27^{Kip1}$ in the retina. In agreement, the major abnormality in $p27^{-/-}$ retinas reside in the photoreceptor layers: the outer granular layer, composed of photoreceptor nuclei, invade the rod and cone layer beyond the outer limiting membrane. Although the precise cause remains to be determined, this seems to be attributable to an inappropriate control of growth, a structural abnormality of photoreceptors, or a loss of integrity in the outer limiting membrane. Considering the enlargement of the thymus, testis, and ovary, organs where $p27^{Kip1}$ is highly expressed, we speculate that the $p27^{Kip1}$ may play an important role in the growth control of photoreceptor cells and that loss of $p27^{Kip1}$ may allow photoreceptors to grow beyond the outer limiting membrane. As far as we know, there is no human genetic disease exactly resembling the retinal abnormality seen in the $p27^{Kip1}$ gene–disrupted mice. Similar changes were reported as senile retinopathy or chemically induced retinopathy in rodents (Lee et al., 1979; Li and Turner, 1988). Thus, $p27^{Kip1}$ gene–ablated mice may be useful as an animal model of retinal dystrophy.

The retinal cells appear to be critically dependent on cell cycle regulation for their development. A disturbance of cell cycle control often results in abnormalities in the retina. Loss of pRb functions was first discovered in a rare human malignancy of the retina, retinoblastoma. pRb regulates the progress of the cell at the late G1 phase of the cell cycle. Anti-mitogenic activity of pRb

is lost by its phosphorylation, which causes a release of factors important for cell cycle progression, such as E2F, from pRb (reviewed by Weinberg, 1995). An increasing body of biochemical evidence indicates that the cyclin D–CDK4/CDK6 complexes phosphorylate pRb to trigger the G1/S transition. Surprisingly, cyclin D1 gene–ablated mice display a dramatic reduction in cell number in the neural retina due to proliferative failure during embryonic development (Sicinski et al., 1995; Fantl et al., 1995). The genetic evidence from cyclin D1–deficient mice supports the idea that pRb is an authentic substrate of a cyclin D–CDK complex and that growth of retinal cells is regulated by pRb and cyclin D. $p27^{Kip1}$ is associated predominantly with cyclin D–CDK4 and shows the ability to inhibit its kinase activity (Toyoshima and Hunter, 1994). Given this connection, one might anticipate the retinal phenotype in $p27^{Kip1}$-deficient animals. Collectively, retinal development appears to be founded on a critical balance among positive and negative regulators of the cell cycle such as pRb, cyclin D–CDK4, and $p27^{Kip1}$. Taken together with the high incidence of pituitary tumors, our study indicates a genetic link among pRb, cyclin D–CDK4, and $p27^{Kip1}$.

Experimental Procedures

Isolation of Mouse $p27^{Kip1}$ cDNA

RNA was extracted from mouse spleen cells by the APCG single-step method (Chomczynski and Sacchi, 1987). The resulting RNA preparation was then used as a template in a cDNA synthesis reaction using $p(dN)_6$ random primers (Invitrogen). This cDNA was used as a template for polymerase chain reaction (PCR) amplification with a set of primers corresponding to the beginning and the end of coding region of $p27^{Kip1}$ (5′-ATGTCAAACGTGAGAGTGTCTAAC-3′ and 5′-TTACGTCTGGCGTCGAAGGCCGGG-3′, respectively). The amplified DNA fragment was subcloned into a pBluescript SKII(+) vector.

Construction of $p27^{Kip1}$ Targeting Vector and Production of Gene-Disrupted Mice

A 129/Sv mouse genomic library (Stratagene) was screened with $p27^{Kip1}$ cDNA as a probe. Of 3×10^6 phages screened, a recombinant phage containing genomic DNA of the $p27^{Kip1}$ locus was isolated. The targeting vector, pMK. KO–neo was constructed by replacement of a 2.5 kb SmaI–SmaI fragment containing the entire $p27^{Kip1}$ coding region with a PGK–neo–polyadenylate (poly[A]) cassette derived from pKJ-1 (Tybulewicz et al., 1991). The targeting vector contained 7.2 kb of homology 5′ and 1.0 kb 3′ of the neomycin-resistance marker. The PGK–tk–poly(A) cassette (Tybulewicz et al., 1991) was ligated into a restriction site in a vector polylinker at the 5′ end of the insert.

The maintenance, transfections, and selections of E14 ES cells were carried out as described previously (Nakayama et al., 1993, 1994). To screen homologous recombinant ES clones, we used cell lysates of the G418- and gancyclovir-resistant clones as templates for PCR amplifications with a $p27^{Kip1}$ flanking primer (5′-GGGCTTTA GAAATAGAGAATGCTG-3′) and a PGK promoter–specific primer (5′-ATGCTCCAGACTGCCTTGGGAAAA-3′). To verify the results of our PCR screening, DNA prepared from PCR-positive ES clones were digested with BamHI, transferred to a nylon membrane (Pall), and then hybridized with the 0.5 kb NdeI–NdeI probe that flanked the 3′ homology region (Figure 2A). Expected sizes for wild-type $p27^{Kip1}$ and mutant $p27^{Kip1}$ are 5.8 kb and 3.8 kb, respectively. Frequency of the homologous recombinations was 15.0% of the double-resistant ES clones.

ES cells heterozygous for the targeted mutation were microinjected into C57BL/6 blastocysts and implanted into pseudopregnant ICR females. The resulting male chimeras were mated with female C57BL/6 mice. The germline transmission of injected ES cells was confirmed by the inheritance of agouti coat color in the F1 animals, and all agouti offspring were tested for the presence of the mutated $p27^{Kip1}$ allele by Southern blot analysis using the same conditions for the detection of homologous recombination events in the ES cells. All mice were maintained in a specific pathogen–free animal facility at Nippon Roche Research Center.

Immunoblot Analysis

Organs from adult C57BL/6 mice were homogenized by a Polytron homogenizer in NP-40 lysis buffer (0.5% NP-40, 50 mM Tris–HCl [pH 8.0], 200 mM NaCl, 20 mM NaF, 20 mM β-glycerophosphate, 0.1 mM Na_3VO_4, 1 mM dithiothreitol, 10 μg/ml leupeptin, 10 KIU/ml aprotinin, 1 mM PMSF). The lysates were incubated on ice for 15 min and then cleared by centrifugation at 10,000 × g. The protein concentration was determined by the Bradford method (protein assay; Bio-Rad). Total lysates (50 μg) from the indicated organs were subjected to SDS–polyacrylamide gel electrophoresis (SDS–PAGE) on a 12% gel and transferred onto Immobilon-P membranes (Millipore). The transferred membrane was soaked in Ponceau-S solution (Sigma) to check the comparable amount of proteins loaded on the gel and the homogeneity of the transfer. The membranes were then probed with a MAb directed against mouse $p27^{Kip1}$ (Transduction Laboratories), β-tubulin (Sigma), or CDK2 (Santa Cruz Biotechnology). The ECL blotting system (Amersham) was used to visualize proteins according to the instructions of the manufacturer. In some cases, we used our own biotinylated anti-$p27^{Kip1}$ MAb and streptavidin conjugated with horseradish peroxidase (Amersham).

Immune Complex Kinase Assay

Thymocytes from the indicated mouse genotypes were suspended at 2.5×10^8 per milliliter in Tween 20 lysis buffer (0.1% Tween 20, 50 mM HEPES [pH 7.5], 150 mM NaCl, 1 mM EDTA, 2.5 mM EGTA, 1 mM dithiothreitol, 10 μg/ml leupeptin, 10 KIU/ml aprotinin, 1 mM PMSF), followed by sonication three times for 3 s on ice. The lysates were cleared by centrifugation at 10,000 × g for 15 min, quickly frozen on powdered dry ice, and stored at −80°C until use. Total lysates (200 μg) were incubated with rabbit anti-CDK2 antibody (Santa Cruz Biotechnology) for 12 hr at 4°C with gentle agitation. Immunocomplexes bound to protein A–Sepharose were collected by centrifugation and washed several times in Tween 20 lysis buffer. For the determination of kinase activity, complexes bound to Sepharose beads were washed once more with 50 mM HEPES (pH 7.5) and suspended in 30 μl of kinase buffer (50 mM HEPES [pH 7.5], 10 mM $MgCl_2$, 1 mM dithiothreitol, 1 μg of histone H1 [Calbiochem], 25 μM unlabeled ATP, and 10 μCi of [γ-^{32}P]ATP [6000 Ci/mmol; Amersham]). The samples were incubated for 30 min at 30°C, denatured in SDS sample buffer, and applied to a 12% SDS–polyacrylamide gel. Dried gels were exposed with BAS 3000 image analyzer for 10 min (Fuji Film).

Histopathological Examinations

For morphological evaluation, tissues were dissected and fixed in 15% buffered formaldehyde, except for the eyes, which were fixed with a 3.1% glutaraldehyde, 2.5% buffered formaldehyde mixture; this fixative was injected into the eyes. Paraffin sections were prepared by standard procedures and stained with hematoxylin and eosin.

Immunohistochemistry

Tissues were dissected, mounted in OCT compound (Miles), and snap frozen in a dry ice–hexane bath. Cryostat sections were cut and incubated with anti-mouse $p27^{Kip1}$ MAb prior to fixation. After this washing, the sections were fixed in methanol and then visualized by anti–mouse immunoglobulin G1 (IgG1) conjugated with fluorescein isothiocyanate (FITC) (Southern Biotech).

Flow Cytometry Analysis

Single cell suspensions were prepared from bone marrow, spleen, thymus, and lymph nodes. For examination of lymphoid development, cells were stained by a combination of anti-CD8-FITC and CD4-phycoerythrin (PE) or anti-B220-FITC and anti-αβTCR-PE. For cell cycle analysis, bromodeoxyuridine (BrdU)-pulsed cells were fixed in 70% ethanol at −20°C overnight and denatured by 2N HCl, 0.5% Triton X-100 for 30 min at room temperature, followed by

neutralization with borax buffer (pH 8.5). Treated cells were subjected to dual color staining with anti-BrdU MAb conjugated with FITC (Becton Dickinson) and 5 μg/ml propidium iodide. All analyses were carried out using the FACSCalibur flow cytometer and Cell Quest software (Becton Dickinson).

Lymphocyte Proliferation Assay

Single cell suspensions from lymph nodes of 4-week-old $p27^{+/+}$, $p27^{+/-}$, and $p27^{-/-}$ mice were prepared and enriched for T cells by magnetic depletion of B cells using rat anti–mouse IgM MAb plus magnetic beads conjugated with sheep anti–rat IgG antibody. The purity of T cells was checked by flow cytometry and was usually over 95%. The purified T cells (10^4) were placed in a culture in 96-well plates coated with anti-CD3 plus anti-CD28 MAbs in the presence or absence of 100 U/ml IL-2. Proliferation was monitored every 24 hr after 48 hr of culture until 148 hr by an XTT colorimetric assay according to the protocol of the manufacturer (Boeringer Mannheim). Absorbance at 490 nm, which correlates with viable cell number, was measured by a model 3550 microplate reader (Bio-Rad).

ERG Examination

Mice were adapted to the dark for 1 hr before testing. Examination was performed as described previously (Olsson et al., 1992; Sicinski et al., 1995). ERGs were recorded by ERG-50 (Kowa) from one eye of each mouse with 0.3 Joule Xenon flash.

Preparation of MEFs and Cell Cultures

Primary MEFs were obtained from 13.5 dpc embryos that were either $p27^{+/+}$ or $p27^{-/-}$ using established procedures (Robertson, 1987). Cells were cultured at 37°C (6% CO_2) in Dulbecco's modified Eagle's medium (DMEM) containing 10% fetal bovine serum (FBS) supplemented with 2 mM L-glutamine, 0.1 mM sodium pyruvate, 0.1 mM MEM nonessential amino acid solution, 100 U/ml penicillin G, 100 μg/ml streptomycin sulfate, and 50 μM 2-mercaptoethanol. For testing G1 arrest due to contact inhibition, the cells were plated in 10 cm culture dishes at a density of 1×10^5 cells per plate. Cells were harvested and counted every 24 hr. BrdU (10 μM; Sigma) was pulsed 30 min before harvesting. For our serum starvation experiments, asynchronous cultures at approximately 50% confluence were washed with phosphate-buffered saline and placed in DMEM containing 0.1% FBS for 48 hr. BrdU (10 μM) was pulsed 30 min before harvesting. For γ-irradiation experiments, G0-synchronized cells obtained by 96 hr serum starvation were exposed to 0 or 20 Gy irradiation and then cultured in DMEM containing 10% FBS and 10 μM BrdU for 24 hr. For PALA experiments, cells were synchronized by serum starvation for 84 hr, and then PALA was added at the indicated concentrations and incubated for 12 hr prior to release into DMEM containing 10% FBS, PALA, and 10 μM BrdU. PALA was obtained from the Drug Synthesis Branch (Developmental Therapeutics Program, Division of Cancer Treatment, National Cancer Institute).

Acknowledgments

Correspondence should be addressed to K. -i. N. We express special thanks to members of the Toxicology and Pathology Department at Nippon Roche Research Center: T. Shiga, Y. Yokoyama, and T. Suguro for making the histopathological sections; N. Uchiya for the electron microscopic examinations; I. Imamura and A. Kawashima for their histopathological evaluations; T. Kubota for the ERG examination; T. Takahashi, M. Satoh, and all of the above for the mouse necropsies; and S. Takizawa for advice regarding hormonal examination. We also thank I. Negishi and Q. Zhang for microinjection; N. Kobayashi and H. Sawa for the photography; J. Johnson for providing us with PALA; M. Enomoto for peer review of general pathology; S. Okisaka for peer review of ophthalmic pathology; R. Asakai and T. Akashi for peer review of ovary and testis pathology; Y. Shinkai, H. Matsushime, H. Takahashi, and H. Toyoshima for the helpful discussions; and J. D. Alvarez and M. Y. Nishikawa for their critical readings of the manuscript. We also thank H. Kiyokawa and A. Koff for communicating results prior to publication.

Received March 11, 1996; revised April 11, 1996.

References

Ahuja, S.S., Paliogianni, F., Yamada, H., Balow, J.E., and Boumpas, D.T. (1993). Effect of transforming growth factor-β on early and late activation events in human T cells. J. Immunol. *150*, 3109–3118.

Brugarolas, J., Chandrasekaran, C., Gordon, J.I., Beach, D., Jacks, T., and Hannon, G.J. (1995). Radiation-induced cell cycle arrest compromised by p21 deficiency. Nature *377*, 552–557.

Bullrich, F., MacLachlan, T.K., Sang, N., Druck, T., Veronese, M.L., Allen, S.L., Chiorazzi, N., Koff, A., Heubner, K., Croce, C.M., and Giordano, A. (1995). Chromosomal mapping of members of the cdc2 family of protein kinases, cdk3, cdk6, PISSLRE, and PITALRE, and a cdk inhibitor, *p27^{Kip1}*, to regions involved in human cancer. Cancer Res. *55*, 1199–1205.

Chan, F.K.M., Zhang, J., Cheng, L., Shapiro, D.N., and Winoto, A. (1995). Identification of human and mouse p19, a novel CDK4 and CDK6 inhibitor with homology to $p16^{ink4}$. Mol. Cell. Biol. *15*, 2682–2688.

Chan, L.C., Kwong, Y.L., Liu, H.W., Lee, C.P., Lie, K.W., and Chan, A.Y. (1992). Deletion 12p in *de novo* acute myeloid leukemia: an association with early progenitor cell. Cancer Genet. Cytogenet. *62*, 47–49.

Chomczynski, P., and Sacchi, N. (1987). Single-step method of RNA isolation by acid guanidinium thiocyanate-phenol-chloroform extraction. Anal. Biochem. *162*, 156–159.

Decker, H.J., Li, F.P., Bixenman, H.A., and Sandberg, A.A. (1990). Chromosome 3 and 12p rearranged in a well-differentiated peritoneal mesothelioma. Cancer Genet. Cytogenet. *46*, 135–137.

Deng, C., Zhang, P., Harper, J.W., Elledge, S.J., and Leder, P. (1995). Mice Lacking $p21^{CIP1/WAF1}$ undergo normal development, but are defective in G1 checkpoint control. Cell *82*, 675–684.

Egerton, M., Scollay, R., and Shortman, K. (1990). Kinetics of mature T-cell development in the thymus. Proc. Natl. Acad. Sci. USA *87*, 2579–2582.

El-Deiry, W.S., Tokino, T., Velculescu, V.E., Levy, D.B., Parsons, R., Trent, J.M., Lin, D., Mercer, W.E., Kinzler, K.W., and Vogelstein, B. (1993). *WAF1*, a potential mediator of p53 tumor suppression. Cell *75*, 817–825.

Fantl, V., Stamp, G., Andrews, A., Rosewell, I., and Dickson, C. (1995). Mice lacking cyclin D1 are small and show defects in eye and mammary gland development. Genes Dev. *9*, 2364–2372.

Fehling, H.J., Krotkova, A., Saint-Ruf, C., and von Boehmer, H. (1995). Crucial role of the pre-T-cell receptor α gene in development of αβ but not γδ T cells. Nature *375*, 795–798.

Firpo, E.J., Koff, A., Solomon, M.J., and Roberts, J.M. (1994). Inactivation of a cdk2 inhibitor during interleukin-2-induced proliferation of human T lymphocytes. Mol. Cell. Biol. *14*, 4889–4901.

Gillett, C., Ranti, V., Smith, R., Fisher, C., Bartek, J., Dickson, C., Barnes, D., and Peters, G. (1994). Amplification and overexpression of cyclin D1 in breast cancer detected by immunohistochemical staining. Cancer Res. *54*, 1812–1817.

Gu, Y., Turck, C.W., and Morgan, D.O. (1993). Inhibition of CDK2 activity *in vivo* by an associated 20K regulatory subunit. Nature *366*, 707–710.

Guan, K.-L., Jenkins, C.W., Li, Y., Nichols, M.A., Wu, X., O'Keefe, C.L., Matera, A.G., and Xiong, Y. (1994). Growth suppression by p18, a $p16^{INK4/MTS1}$ and $p14^{INK4/MTS2}$-related CDK6 inhibitor, correlates with wild-type pRb function. Genes Dev. *8*, 2939–2952.

Halevy, O., Novitch, B.G., Spicer, D.B., Skapek, S.X., Rhee, J., Hannon, G.J., Beach, D., and Lassar, A.B. (1995). Correlation of terminal cell cycle arrest of skeletal muscle with induction of p21 by MyoD. Science *267*, 1018–1021.

Hannon, G.J., and Beach, D. (1994). $p15^{INK4B}$ is a potential effector of TGF-β-induced cell cycle arrest. Nature *371*, 257–261.

Harper, J.M., Adami, G.R., Wei, N., Keyomarsi, K., and Elledge, S.J. (1993). The p21 Cdk-interacting protein Cip1 is a potent inhibitor of G1 cyclin–dependent kinases. Cell *75*, 805–816.

Hirai, H., Roussel, M.F., Kato, J.-Y., Ashmun, R.A., and Sherr, C.J. (1995). Novel Ink4 proteins, p19 and p18, are specific inhibitors of

cyclin D-dependent kinases CDK4 and CDK6. Mol. Cell. Biol. *15*, 2672–2681.

Hunter, T., and Pines, J. (1994). Cyclins and cancer II: cyclin D and CDK inhibitors come of age. Cell *79*, 573–582.

Hussussian, C.J., Struewing, J.P., Goldstein, A.M., Higgins, P.A.T., Ally, D.S., Sheahan, M.D., Clark, W.H., Jr., Tucker, M.A., and Dracopoli, N.C. (1994). Germline *p16* mutations in familial melanoma. Nature Genet. *8*, 15–21.

Jacks, T., Fazeli, A., Schmitt, E.M., Bronson, R.T., Goodell, M.A., and Weinberg, R.A. (1992). Effects of an *Rb* mutation in the mouse. Nature *359*, 295–300.

Jiang, H., Su, Z.-Z., Collart, F., Huberman, E., and Fisher, P. (1994). Induction of differentiation in human promyelocytic HL60 leukemia cells activates p21$^{WAF1/CIP1}$ expression in the absence of p53. Oncogene *9*, 3397–3406.

Kawamata, N., Morosetti, R., Miller, C.W., Park, D., Spirin, K.S., Nakamaki, T., Takeuchi, S., Hatta, Y., Simpson J., Wilczynski, S., Lee, Y.Y., Bartram, C.R., and Koeffler, H.P. (1995). Molecular analysis of the cyclin-dependent kinase inhibitor gene *p27/Kip1 in human malignancies. Cancer Res. 55*, 2266–2269.

Kehrl, J.H., Wakefield, L.M., Roberts, A.B., Jakowlew, S.B., Sporn, M.B., and Fauci, A.S. (1986). Production of transforming growth factor β by human lymphocytes and its potential role in the regulation of the T cell growth. J. Exp. Med. *163*, 1037–1050.

Lammie, G.A., Fantl, V., Smith, R., Schuuring, E., Brookes, S., Michalides, R., Dickson, C., Arnold, A., and Peters, G. (1991). D11S128, a putative oncogene on chromosome 11q13 is amplified and expressed in squamous cell and mammary carcinomas and linked to BCL-1. Oncogene *6*, 439–444.

Lee, E.Y.-H.P., Chang, C.-Y., Hu, N., Wang, Y.-C.J., Lai, C.-C., Herrup, K., Lee, W.-H., and Bradley, A. (1992). Mice deficient for Rb are nonviable and show defects in neurogenesis and haematopoiesis. Nature *359*, 288–294.

Lee, K.P., Gibson, J.R., and Sherman, H. (1979). Retinipathic effects of 2-aminoxy propionic acid derivatives in the rat. Toxicol. Appl. Pharmacol. *51*, 219–232.

Lee, M.-H., Reynisdóttir, I., and Massagué, J. (1995). Cloning of p57^{KIP2}, a cyclin-dependent kinase inhibitor with unique domain structure and tissue distribution. Genes Dev. *9*, 639–649.

Li, I., and Turner, J.E. (1988). Inherited retinal degeneration in the RCS rat: prevention of photoreceptor degeneration by pigment epithelial cell transplantation. Exp. Eye Res. *47*, 911–917.

Mansour, S., Thomas, K.R., and Capecchi, M.R. (1988). Disruption of the proto-oncogene int-2 in mouse embryo-derived stem cells: a general strategy for targeting mutations to non-selectable genes. Nature *336*, 348–352.

Matsuoka, S., Edwards, M., Bai, C., Parker, S., Zhang, P., Baldini, A., Harper, J.W., and Elledge, S.J. (1995). p57^{KIP2}, a structurally distinct member of the p21^{CIP1} Cdk-inhibitor family, is a candidate tumor suppressor gene. Genes Dev. *9*, 650–662.

Mombaerts, P., Clarke, A.R., Rudnicki, M.A., Iacomini, J., Itohara, S., Lafaille, J.J., Wang, L., Ichikawa, Y., Jaenisch, R., Hooper, M.L., and Tonegawa, S. (1992). Mutations in T-cell antigen receptor genes α and β block thymocyte development at different stages. Nature *360*, 225–231.

Mori, T., Miura, K., Aoki, T., Nishimura, T., Mori, S., and Nakamura, Y. (1994). Frequent somatic mutation of the MTS1/CDK4I (multiple tumor suppressor/cyclin-dependent kinase 4 inhibitor) gene in esophageal squamous cell carcinoma. Cancer Res. *54*, 3396–3397.

Morosetti, R., Kawamata, N., Gombart, A.F., Miller, C.W., Hatta, Y., Hirama, T., Said, J.W., Tomonaga, M., and Koeffler, H.P. (1995). Alterations of the p27^{Kip1} gene in non-Hodgkin's lymphomas and adult T-cell leukemia/lymphoma. Blood *86*, 1924–1930.

Motokura, T., Bloom, T., Kim, H.G., Juppner, H., Ruderman, J.V., Kronenberg, H.M., and Arnold, A. (1991). A novel cyclin encoded by a *bcl*-linked candidate oncogene. Nature *350*, 512–515.

Nakayama, K.-i., Nakayama, K., Negishi, I., Kuida, K., Shinkai, Y., Louie, M.C., Fields, L.E., Lucas, P.J., Stewart, V., Alt, F.W., and Loh, D.Y. (1993). Disappearance of the lymphoid system in Bcl-2 homozygous mutant chimeric mice. Science *261*, 1584–1588.

Nakayama, K.-i., Nakayama, K., Negishi, I., Kuida, K., Louie, M.C., Kanagawa, O., Nakauchi, H., and Loh, D.Y. (1994). Requirement for CD8 β chain in positive selection of CD8-lineage T cells. Science *263*, 1131–1133.

Noda, A., Ning, Y., Venable, S.F., Pereila-Smith, O.M., and Smith, J.R. (1994). Cloning of senescent cell-derived inhibitors of DNA synthesis using an expression screen. Exp. Cell Res. *211*, 90–98.

Noguchi, E., Sekiguchi, T., Yamashita, K., and Nishimoto, T. (1993). Molecular cloning and identification of two types of hamster cyclin-dependent kinases: cdk2 and cdk2L. Biochem. Biophys. Res. Commun. *197*, 1524–1529.

Nourse, J., Firpo, E., Flanagan, W.M., Coats, S., Polyak, K., Lee, M.-H., Massagué, J., Crabtree, G.R., and Roberts, J.M. (1994). Interleukin-2-mediated elimination of the p27^{Kip1} cyclin-dependent kinase inhibitor prevented by rapamycin. Nature *372*, 570–573.

Olsson, J.E., Gordon, J.W., Pawlyk, B.S., Roof, D., Hayes, A., Molday, R.S., Mukai, S., Cowley, G.S., Berson, E.L., and Dryja, T.P. (1992). Transgenic mice with a rhodopsin mutation (Pro23His): a mouse model of autosomal dominant retinitis pigmentosa. Neuron *9*, 815–830.

Pagano, M., Tam, S.W., Theodoras, A.M., Beer-Romero, P., Del Sal, G., Chau, V., Yew, P.R., Draetta, G.F., and Rolfe, M. (1995). Role of the ubiquitin-proteasome pathway in regulating abundance of the cyclin-dependent kinase inhibitor p27. Science *269*, 682–685.

Parker, S.B., Eichele, G., Zhang, P., Rawls, A., Sands, A.T., Bradley, A., Olson, E.N., Harper, J.W., and Elledge, S.J. (1995). p53-independent expression of p21^{Cip1} in muscle and other terminally differentiating cells. Science *267*, 1024–1027.

Pietenpol, J.A., Bohlander, S.K., Sato, Y., Papadopoulos, N., Liu, B., Friedman, C., Trask, B.J., Roberts, J.M., Kinzler, K.W., Rowley, J.D., and Vogelstein, B. (1995). Assignment of the human *p27^{Kip1}* gene to 12p13 and its analysis in leukemias. Cancer Res. *55*, 1206–1210.

Polyak, K., Kato, J.-y., Solomon, M.J., Sherr, C.J., Massagué, J., Roberts, J.M., and Koff, A. (1994a). p27^{Kip1}, a cyclin-Cdk inhibitor, links transforming growth factor-β and contact inhibition to cell cycle arrest. Genes Dev. *8*, 9–22.

Polyak, K., Lee, M.H., Erdjument-Bromage, H., Tempst, P., and Massagué, J. (1994b). Cloning of p27^{KIP1}, a cyclin-dependent kinase inhibitor and potential mediator of extracellular antimitogenic signals. Cell *78*, 59–66.

Ponce-Castaneda, M.V., Lee, M.-H., Latres, E., Polyak, K., Lacombe, L., Montgomery, K., Mathew, S., Krauter, K., Sheinfeld, J., Massagué, J., and Cordon-Cardo, C. (1995). *p27^{Kip1}*: chromosomal mapping to 12p12-12p13.1 and absence of mutations in human tumors. Cancer Res. *55*, 1211–1214.

Reynisdóttir, I., Polyak, K., Iavarone, A., and Massagué, J. (1995). Kip/Cip and Ink4 Cdk inhibitors cooperate to induce cell cycle arrest in response to TGF-β. Genes Dev. *9*, 1831–1845.

Robertson, E.J. (1987). Embryo-derived stem cell lines. In Teratocarcinomas and Embryonic Stem Cells: A Practical Approach, E.J. Robertson, ed. (Oxford: IRL Press), pp. 71–112.

Serrano, M., Hannon, G.J., and Beach, D. (1993). A new regulatory motif in cell cycle control causing specific inhibition of cyclin D/CDK4. Nature *366*, 704–707.

Sherr, C.J. (1994). G1 phase progression: cycling on cue. Cell *79*, 551–555.

Sherr, C.J., and Roberts, J.M. (1995). Inhibitors of mammalian G1 cyclin-dependent kinases. Genes Dev. *9*, 1149–1163.

Shinohara, M., El-Deiry, W.S., Wada, M., Nakamaki, T., Takeuchi, S., Yang, R., Chen, D.L., Vogelstein, B., and Koeffler, H.P. (1994). Absence of *WAF1* mutations in a variety of human malignancies. Blood *84*, 3781–3784.

Shull, M.M., Ormsby, I., Kier, A.B., Pawlowski, S., Diebold, R.J., Yin, M., Allen, R., Sidman, C., Proetzel, G., Calvin, D., Annunziata, N., and Doetschman, T. (1992). Targeted disruption of the mouse transforming growth factor-β1 gene results in multifocal inflammatory disease. Nature *359*, 693–699.

Sicinski, P., Donaher, J.L., Parker, S.B., Li, T., Fazeli, A., Gardner, H., Haslam, S.Z., Bronson, R.T., Elledge, S.J., and Weinberg, R.A. (1995). Cyclin D1 provides a link between development and oncogenesis in the retina and breast. Cell *82*, 621–630.

Steinman, R.A., Hoffman, B., Iro, A., Guillouf, C., Liebermann, D.A., and El-Houseini, M.E. (1994). Induction of p21(*WAF1/CIP1*) during differentiation. Oncogene *9*, 3389–3396.

Swyryd, E.A., Seaver, S., and Stark, G.R. (1974). N-(phosphonacetyl)-L-aspartate, a potent transition state analog inhibitor of aspartate transcarbamylase, blocks proliferation of mammalian cells in culture. J. Biol. Chem. *249*, 6945–6950.

Toyoshima, H., and Hunter, T. (1994). p27, a novel inhibitor of G1 cyclin–Cdk protein kinase activity, is related to p21. Cell *78*, 67–74.

Tybulewicz, V.L., Crawford, C.E., Jackson, P.K., Bronson, R.T., and Mulligan, R.C. (1991). Neonatal lethality and lymphopenia in mice with a homozygous disruption of the c-abl proto-oncogene. Cell *65*, 1153–1163.

Wahl, S.M., McCartney-Francis, N., and Mergenhagen, S.E. (1989). Inflammatory and immunomodulatory roles of TGF-β. Immunol. Today *10*, 258–261.

Weinberg, R.A. (1995). The retinoblastoma protein and cell cycle control. Cell *81*, 323–330.

Williams, B.O., Schmitt, E.M., Remington, L., Bronson, R.T., Albert, D.M., Weinberg, R.A., and Jacks, T. (1994). Extensive contribution of Rb-deficient cells to adult chimeric mice with limited histopathological consequences. EMBO J. *13*, 4251–4259.

Xiong, Y., Hannon, G.J., Zhang, H., Casso, D., Kobayashi, R., and Beach, D. (1993). *p21* is a universal inhibitor of cyclin kinases. Nature *366*, 701–704.